Atomistic Mechanism of Broadband Emission in Metal Halide Perovskites

Xiaoming Wang,[†] Weiwei Meng,[†,‡] Weiqiang Liao,[§] Jianbo Wang,[‡] Ren-Gen Xiong,[§] and Yanfa Yan[,†]*

[†]Department of Physics and Astronomy, and Wright Center for Photovoltaic Innovation and Commercialization, The University of Toledo, Toledo, OH 43606, United States

[‡]School of Physics and Technology, Center for Electron Microscopy, MOE Key Laboratory of Artificial Micro-and Nano-structures, and Institute for Advanced Studies, Wuhan University, Wuhan 430072, China

[§]Ordered Matter Science Research Center, Southeast University, Nanjing 211189, China

AUTHOR INFORMATION

Corresponding Author

*yanfa.yan@utoledo.edu

ABSTRACT Broadband emission is attributed to the formation of self-trapped excitons (STEs) due to the strong electron-phonon coupling. Interestingly, it has been observed in only certain three-dimensional and low-dimensional metal halide perovskites. Here, we show by density-functional theory calculation that a low electronic dimensionality is a prerequisite for the formation

of STE and, therefore, broadband emission. We further show that multiple STE structures exist in each perovskite exhibiting broadband emission. However, only the STE with Jahn-Teller like octahedral distortion is mainly responsible for the observed broadband emission, though it may not be the lowest energy structure. Our results provide important insights for designing perovskite materials for broadband emissions with preferred chromaticity coordinator or color temperature.

TOC GRAPHICS

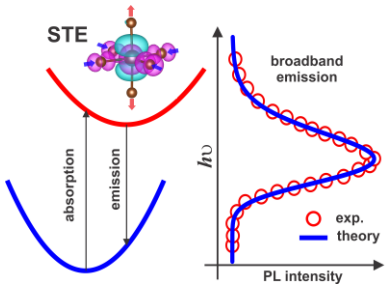

KEYWORDS self-trapped exciton, broadband emission, first-principles, halide perovskites

Metal halide perovskites have been attracting great attention during the past few years as emerging optoelectronic materials in solar cells and light emitting devices (LEDs).[1] While metal halide perovskite solar cells have enjoyed rapid progress in record power conversion efficiency, metal halide perovskite LEDs have also shown steady progress in light emitting quantum efficiencies. Perovskite LEDs include both narrowband single color light emission and broadband white light emission. In LED applications, the broadband emission covering the entire visible spectrum has recently drawn intensive attention, since such white light emission can be realized in single material. Broadband emission is commonly attributed to the formation of self-trapped excitons (STEs)[2–4] due to the strong electron-phonon coupling. Therefore, it is rather intuitive to expect that

three-dimensional (3D) perovskites should emit narrowband lights and lower dimensional perovskites should emit broadband lights. In the perovskite community, the structural dimensionality usually refers to the metal halide octahedral connections. Therefore, 3D perovskite means the octahedral connections extend over all the three directions in space, e.g., ABX_3 (A = Cs, MA, FA; B = Pb, Sn; X = Cl, Br, I). If the octahedral connection along one direction is broken, then we get the so-called 2D layered perovskites. Similarly, we have 1D chained and 0D isolated perovskites. Indeed, many 3D perovskites demonstrate excellent narrow photoluminescence (PL) with full width at half maximum (FWHM) less than 50 nm. This narrowband feature is due to free-exciton emission, the peak of which is located near the optical absorption onset. Interestingly, however, not all 3D perovskites show narrowband emission. For example, 3D $CsPbCl_3$ (low-symmetry phase) and $(C_5H_{14}N_2)PbBr_3$ show very broad emission with FWHM of 187 nm and 570 nm, respectively, and a large Stokes shift.[5,6] Another group of 3D perovskites with broadband emission is double perovskite $A_2B(I)B'(III)X_6$, examples of which are $Cs_2AgInCl_6$[7–10], $Cs_2NaInCl_6$[7], $Cs_2NaBiCl_6$[11]. Some 2D perovskites show broadband emission,[2,3,6,12–25] see Table S1. But still not all the 2D perovskites always show broadband emission,[19,23,25] which is believed to have a strong correlation with the in-plane and out-of-plane octahedral distortions.[12,23,25] Further reducing the dimensionality to 1D and 0D, all the reported perovskites show broadband emission.[4,6,26–28] It seems that a simple correlation between the structural dimensionality and the broadband emission does not exist, see Table S1. From mechanistic point of view, although it is widely believed that the origin of the broadband emission is due to STEs, however, rigorous evidence is still lacking.

In this work, we resolve this issue by theoretically evaluating the STE formation and give a clear evidence of the atomistic mechanism of the broadband emission. We show that it is the

electronic dimensionality rather than the structural dimensionality that determines the type of emission – a low electronic dimensionality is prerequisite for the formation of STE and, therefore, broadband emission. We further show that to exhibit strong broadband emission, the responding STE must have Jahn-Teller like octahedral distortion. A perovskite may emit weak broadband light is the responding STE has a non Jahn-Teller like octahedral distortion. Our results provide important insights for tuning the quantum yield and chromaticity coordinator of broadband emissions in metal halide perovskites.

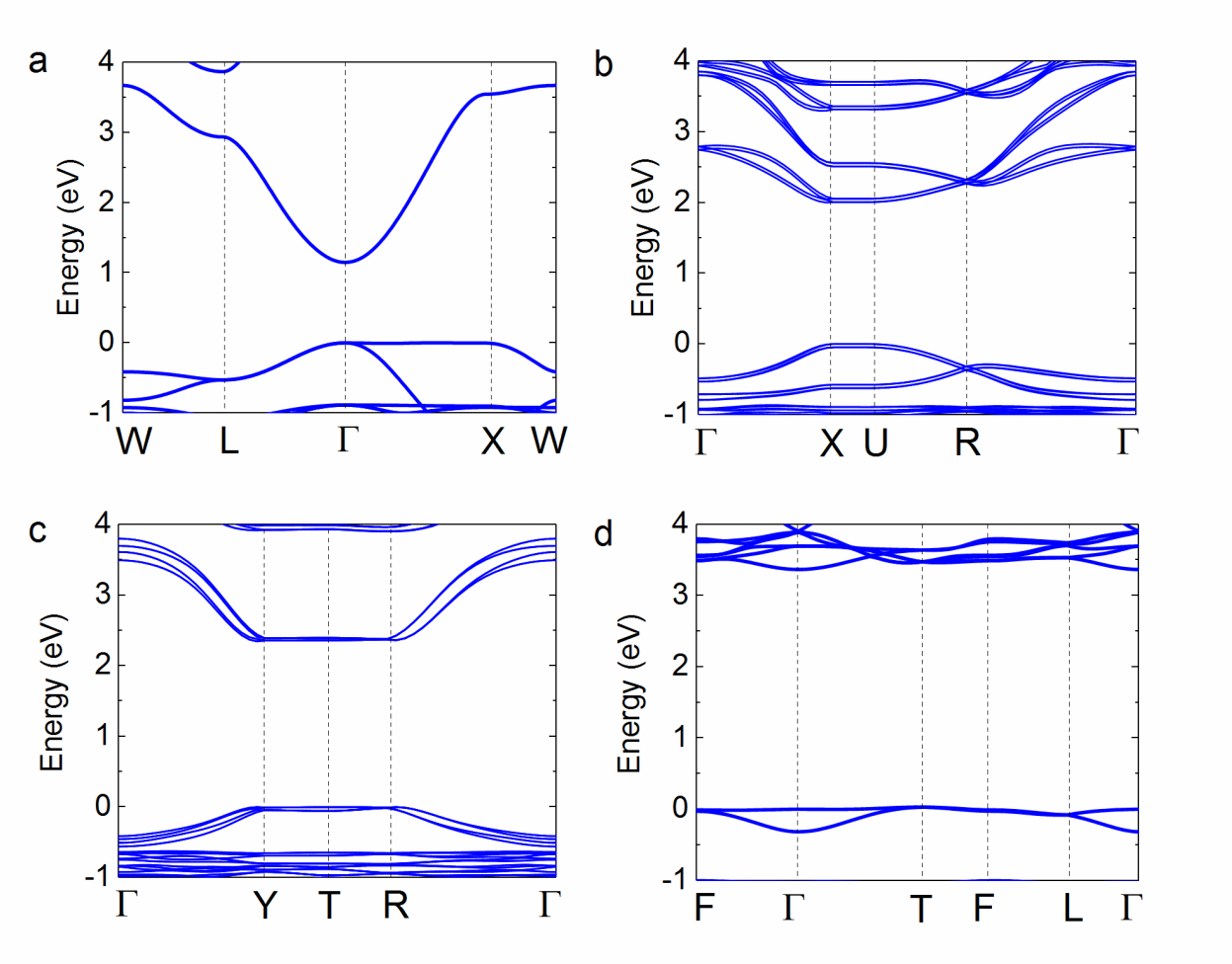

Figure 1. DFT band structures of (a) 3D $Cs_2AgInCl_6$ (b) 2D (NMEDA)$PbBr_4$ (c) 1D $C_4N_2H_{14}PbBr_4$ (d) 0D Cs_4SnBr_6. Spin-orbit coupling is included for Pb-base perovskites. The

energy of the valence band maximum is set to zero. The band gap is underestimated with the PBE functional.

We first elucidate the origin of the broadband emission from the viewpoint of electronic structures. For the excitons to be able to self-trap, either photo-generated electrons or holes, or both must not be very delocalized, i.e., the effective mass of either or both of the carriers must not be extremely light. In other word, a low electronic dimensionality[29], which describes the degree of orbital overlaps, is a prerequisite for formation of STEs and, therefore, the broadband emission. The electronic dimensionality of a semiconductor can be evaluated from the calculation of its electronic properties. For example, Figure 1a shows the calculated band structure of $Cs_2AgInCl_6$., which has a 3D structural dimensionality. It shows large conduction bandwidth and dispersive band edge, which serves as the example of high electronic dimensionality. However, the top valence band is contributed from the [$AgCl_6$] octahedra. Despite the 3D crystalline structure, the orbital overlap between different [$AgCl_6$] octahedra is broken by the neighboring [$InCl_6$] octahedra, resulting in reduced electronic dimensionality. Hence, we see low electronic dimensionality for the hole of $Cs_2AgInCl_6$, i.e., the valence band edge is completely flat in the Γ to X direction (Fig. 1a). The heavy hole can be easily self-trapped and then attracts the surrounding electron to form STE. Figures 1b, c, and d show the calculated band structures of the 2D (NMEDA)$PbBr_4$ [NMEDA = N^1-methylethane-1,2-diammonium][19], 1D $C_4N_2H_{14}PbBr_4$[4] and 0D Cs_4SnBr_6[27] halide perovskites, respectively. Flat bands can be clearly seen in low-dimensional perovskites due to the broken of the octahedral connection networks. Compared with that of the conduction band of $Cs_2AgInCl_6$, the bandwidths of the low-dimensional perovskites are shrunk. Note that, the reduction of the bandwidth along only one direction is not enough for the STE formation. For instance, the top valence bandwidths of both the two (100) layered perovskites,

namely, (BDA)$PbBr_4$ and (NMPDA)$PbBr_4$ [BDA = butane-1,4-diammonium; NMPDA = N^1-methylpropane-1,3-diammonium], along the cross-plane direction are nearly zero. However, the former shows broadband emission while the latter is not.[19,25] Comparing the band structures of the two compounds, see Figure S1, we find that the in-plane bandwidth of (BDA)$PbBr_4$ is further reduced due to the out-of-plane octahedral distortions. Therefore, the in-plane confined exciton tends to be further localized in (BDA)$PbBr_4$ while delocalized in (NMPDA)$PbBr_4$. With similar arguments, the (110)-oriented 2D perovskites are easier for the STE formation than (100) counterparts. Hence, it is necessary for the electronic dimensionality to be reduced in all directions to form STEs. We see that all the above mentioned materials with broadband emission share the common feature of low electronic dimensionality. Upon photoexcitations, the free charge carriers with heavy effective mass tend to be confined in the crystal lattice which is vibrating due to thermal excitations, also known as phonons. For materials with strong electron-phonon coupling, the free charge carriers interact intensively with phonons to form polarons, or self-trapped holes or electrons. The electron and hole polarons can further bind each other Coulombically to form STEs. The free exciton self-traps once the self-trapping energy is larger than half the bandwidth.[30] It is noted that a low electronic dimensionality is just a prerequisite for the formation of STEs, not all semiconductors with low electronic dimensionality will always lead to broadband emission. A large trapping energy of STE can only result from soft atomic bonding, for which the lattice deformation energy E_d is not enormous. Such information can be obtained from calculating the exciton-phonon coupling.

Table 1. Electronic and optical properties of STEs in metal halide perovskites.

		$Cs_2AgInCl_6$	(NMEDA)$PbBr_4$		$C_4N_2H_{14}PbBr_4$			Cs_4SnBr_6	
E_g (eV)		3.27	3.82		4.20			5.01	
E_b (eV)		0.05	0.60		0.84			1.25	
E_{opt} (eV)	theory	3.22	3.22		3.36			3.76	
	exp.	3.3[a]	3.20[b]		3.27[c]			3.65[d]	
STE type		STE1	STE1	STE2	STE1	STE2A	STE2B	STE1	STE2
$\|\boldsymbol{\mu}\|^2$ (e^2 $Bohr^2$)		0	0.55	0.01	0.86	0.04	0.03	1.87	0.04
E_{st} (eV)		0.53	0.55	0.58	0.42	0.33	0.28	0.72	0.79
E_d (eV)		0.67	0.51	1.15	0.50	1.02	1.02	0.77	2.46
E_{PL} (eV)	theory	1.82	2.16	1.55	2.44	2.01	2.06	2.27	0.51
	exp.	2.04[a]	2.21[b]		2.36[c]			2.30[d]	
$\hbar\Omega_g$(meV)		18.3	4.92	6.41	7.01	9.89	8.02	6.59	7.11
$\hbar\Omega_e$ (meV)		17.4	6.70	7.62	7.43	8.80	7.57	6.72	6.39
S_g		37	104	179	71	103	135	117	346
S_e		30	82	76	57	38	37	107	124
τ (fs)		238	617	543	557	470	546	615	647

[a]Ref.[9]; [b]Ref.[19]; [c]Refs.[4]; [d]Ref.[27].

E_g, E_b, E_{opt}, E_{st}, E_d, E_{PL} are the bandgap, exciton binding energy, optical bandgap, self-trapping energy, lattice deformation energy, and emission energy, respectively. Ω is phonon frequency and S Huang-Rhys factor, where g for ground state and e for excited state. τ is the exciton self-trapping time. $|\boldsymbol{\mu}|^2$ is the square modulus of transition dipole moment.

We now evaluate the STE structures that are responsible for the experimentally observed broadband emissions. We probe the exciton-phonon coupling by relaxing the lattice initiated at the free exciton state. We find that there are two types of STE structures in metal halide perovskites, i.e., Jahn-Teller like distortion (STE1) and non Jahn-Teller like distortion (STE2). We further find that it is the STE1 that accounts for the most observed broadband emission. While some perovskite may have only one STE structures, some others may contain both STE structures. The electronic and optical properties of STEs in metal halide perovskites are listed in Table 1. The structural 3D

$Cs_2AgInCl_6$ forms STE1 with elongation of the two axial Ag-Cl bonds and contraction of the four equatorial Ag-Cl bonds.[7] The hole is localized within one single [$AgCl_6$] octahedron, whereas the electron is quite spread, see Figure S2. This is consistent with the low and high electronic dimensionality of the hole and electron, respectively, as shown by the band structure in Figure 1a. The calculated PL spectrum of the STE emission agrees very well with experiment[7], confirming the STE as the origin of the observed broadband emission. The structural 3D $Cs_2NaInCl_6$, however, forms the STE2 structure.[7]

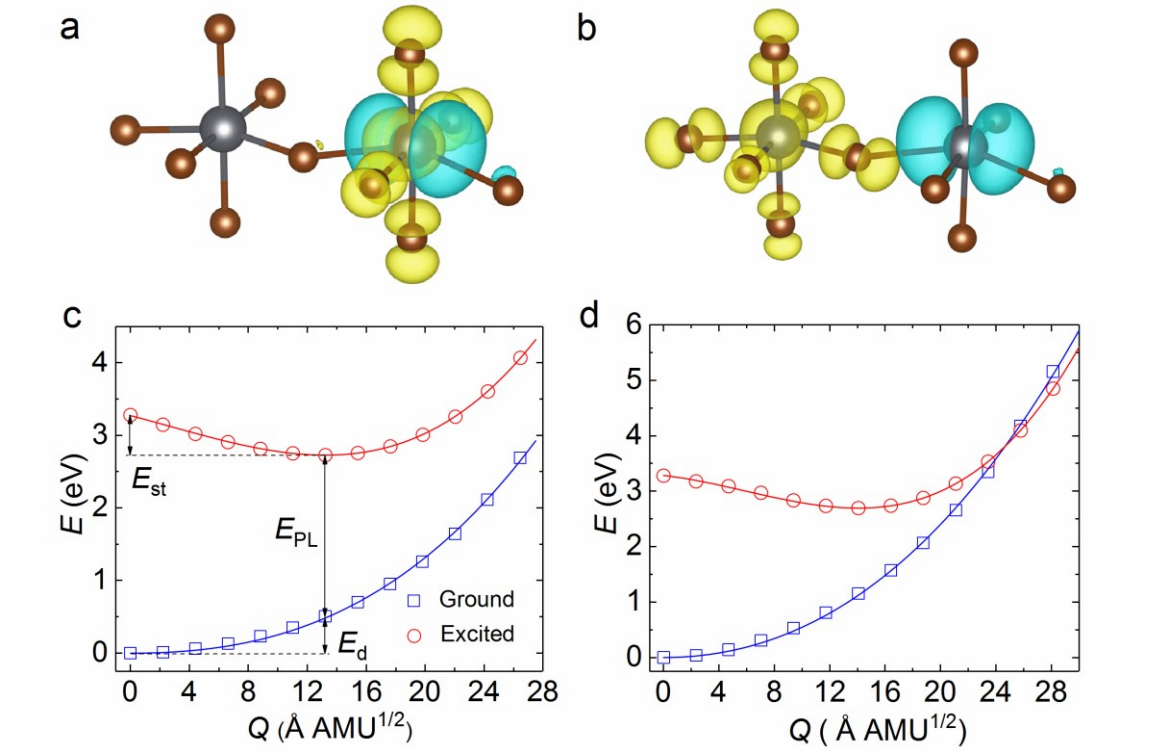

Figure 2. (a) STE1 and (b) STE2 in (NMEDA)PbBr4. The STEs are shown by combination of electron (cyan) and hole (yellow) orbital densities. (c) and (d) are the corresponding configuration coordinate diagrams for STE1 and STE2, respectively. E_{st}, E_{PL}, and E_d are the energies of self-trapping, emission, and lattice deformation, respectively. Symbols are the calculated data while the lines are fitting curves.

Both STE1 and STE2 are found in 2D (NMEDA)$PbBr_4$, as shown in Figures 2a and b. The structure of STE1 is quite similar to the Jahn-Teller STE of $Cs_2AgInCl_6$, namely, the [$PbBr_6$] octahedron with elongation of the axial bonds and contraction of the equatorial bonds. STE1 is mainly localized in one [$PbBr_6$] octahedron, whereas STE2 occupies two neighboring [$PbBr_6$] octahedra with one trapping the hole by contraction of the six Pb-Br bonds and the other one trapping the electron by elongation of the two Pb-Br bonds in the octahedral connecting direction. Note that it is along the linear other than corrugated octahedral connecting direction in the 2D plane that the STE2 forms. From the STE orbitals shown in Figure 2, it is obvious that the electron-hole orbital overlap of STE2 is dramatically reduced, which leads to a much smaller transition dipole moment square $|\boldsymbol{\mu}|^2$, i.e., 0.01 a.u. compared to 0.55 a.u. of STE1. The energetics of the STE formation is depicted by the configuration coordinate (cc) diagrams[31], as shown in Figures 2c and d for STE1 and STE2, respectively. The self-trapping energy, E_{st}, the energy difference between the free exciton and STE, of STE2 is only 30 meV lower than that of STE1, whereas the lattice deformation energy, E_d, the change of the ground-state energy due to the STE formation, of STE2 is 0.64 eV larger than that of STE1. This is because two Pb-Br bonds need to be elongated to trap an electron for both STE1 and STE2 but two more Pb-Br bonds need to be contracted to trap a hole for STE2. It is well-known that STE forms due to strong electron-phonon coupling which can be deduced from the large Huang-Rhys factors[32], $S_g = E_d/\hbar\Omega_g$ for ground state, $S_e = E_{st}/\hbar\Omega_e$ for excited state, where Ω is the phonon frequency obtained by fitting the cc diagrams, as shown in Table 1. The exciton self-trapping time $\tau = 2\pi/\Omega_e$ is evaluated to be 617 fs and 543 fs for STE1 and STE2, respectively. These numbers are consistent with the ultrafast spectroscopic data[2]. One obvious distinction of the two cc diagrams is that the ground state and excited state cross for STE2, which indicates a pathway for non-radiative transition. The calculated PL spectra of the STEs

compared with experimental data are shown in Figure 3. The PL intensity of STE2 is two orders of magnitude smaller than that of STE1, implying the weakness of the radiative emission of STE2. The excellent agreement with the experimental PL line shape clearly evidences the origin of the broadband emission from the Jahn-Teller like STE in (NMEDA)$PbBr_4$.

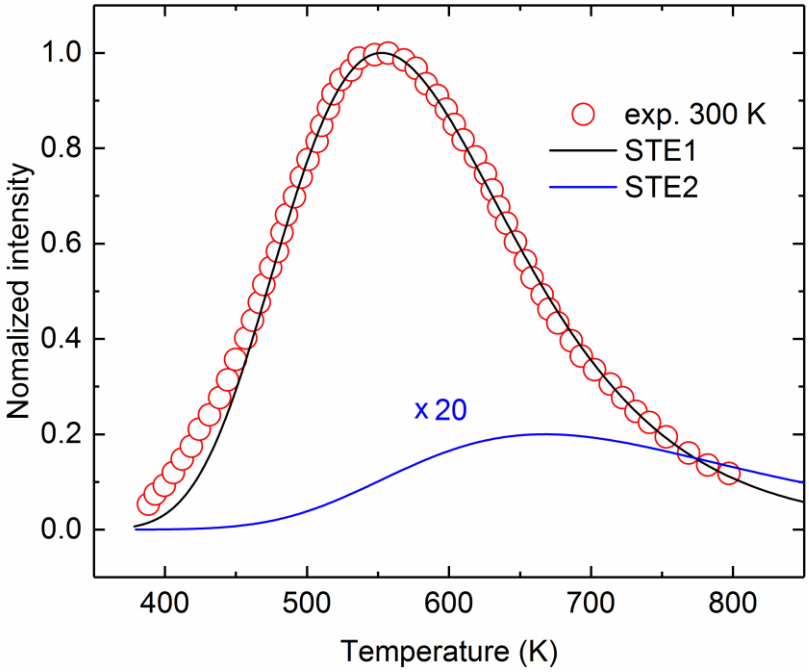

Figure 3. Theoretical photoluminescence spectra of STEs in (NMEDA)$PbBr_4$ compared with experiment[2].

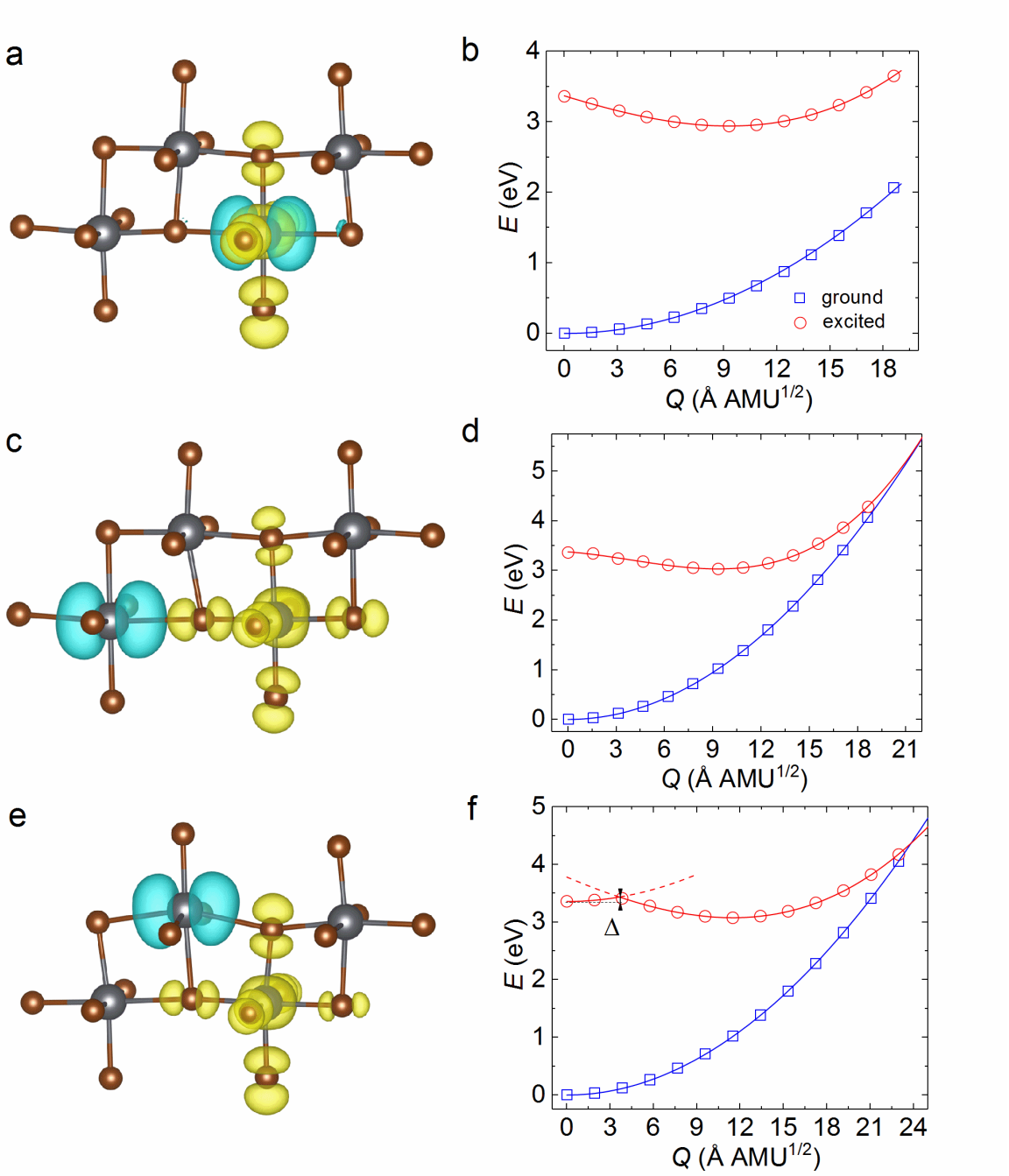

Figure 4. (a)(c)(e) Three STEs in $C_4N_2H_{14}PbBr_4$ and (b) (d) (f) the corresponding configuration coordinate diagrams. Same caption details as Figure 2.

Similar to the 2D case, we find that the STEs of 1D metal halide perovskite can also be Jahn-Teller like (STE1) or non Jahn-Teller like (STE2), as shown in Figure 4. For the STE2, the two

[$PbBr_6$] units can be in one octahedral chain (STE2A) or two separate edge sharing chains (STE2B). Contrary to the 2D perovskite, the STE1 is most stable. STE1 and STE2B have also been observed in previous work[28] but with reversed energy order possibly because of the different halogens used. Both STE2A and STE2B have intersections in the cc diagrams as shown in Figures 4d and f, indicating that these two STEs are non-radiative recombination centers. Moreover, STE2B demonstrates a self-trapping barrier of $\Delta = 50$ meV. Therefore, thermal excitation is needed to activate STE2B, implying less population of STE2B compared with other two STEs. Figure 5 shows the calculated PL spectra. The PL intensities of STE2A and STE2B are much smaller than that of STE1 and should be hardly observable in experiment. The excellent agreement of the PL spectrum of STE1 compared with experiment again confirms the Jahn-Teller like STE as the origin of the observed broadband emission.

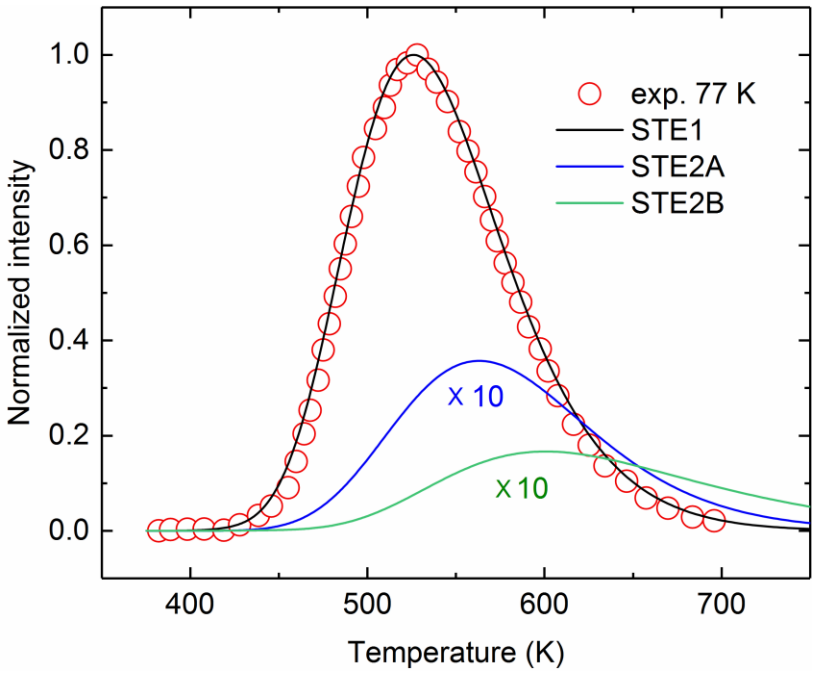

Figure 5. Theoretical photoluminescence spectra of STEs in $C_4N_2H_{14}PbBr_4$ compared with experiment[4].

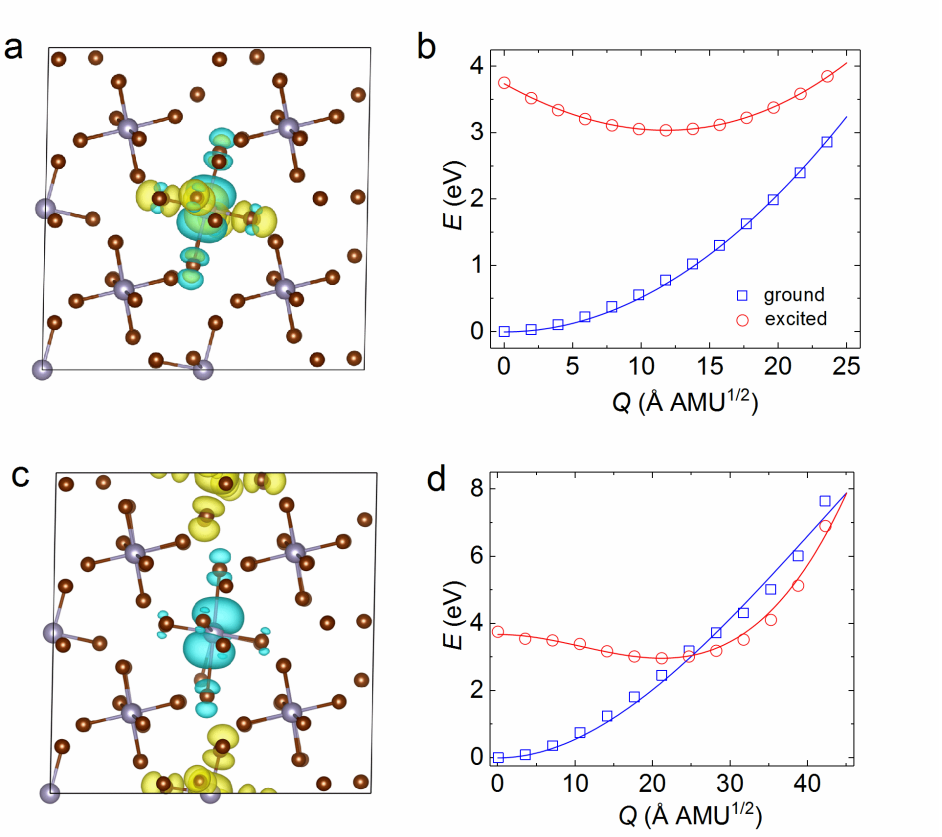

Figure 6. (a) STE1 (c) STE2 of Cs_4SnBr_6 and the corresponding configuration coordinate diagrams in (b) and (d).

The STE1 also forms in 0D Cs_4SnBr_6, as shown in Figure 6a. Due to the octahedral isolation, the STE is much confined compared with that of 1D and 2D perovskites, which enhances the electron-hole overlap significantly, as shown by the larger transition dipole moment in Table 1. The calculated PL spectrum shown in Figure 7 also agrees with experiment[27]. Like those in 2D and 1D perovskites, the STE2 in Cs_4SnBr_6 can also form by occupying two octahedra. STE2 is calculated to be 70 meV more stable than STE1. The cc diagram of STE2, Figure 6d, shows an intersection of the ground state and excited state nearby the STE configuration, which means that

the non-radiative transition barrier is rather small. This combined with the small transition dipole moment makes STE2 almost unobservable in experiment. Therefore, again the broadband emission of Cs_4SnBr_6 is originated from the Jahn-Teller like STE1.

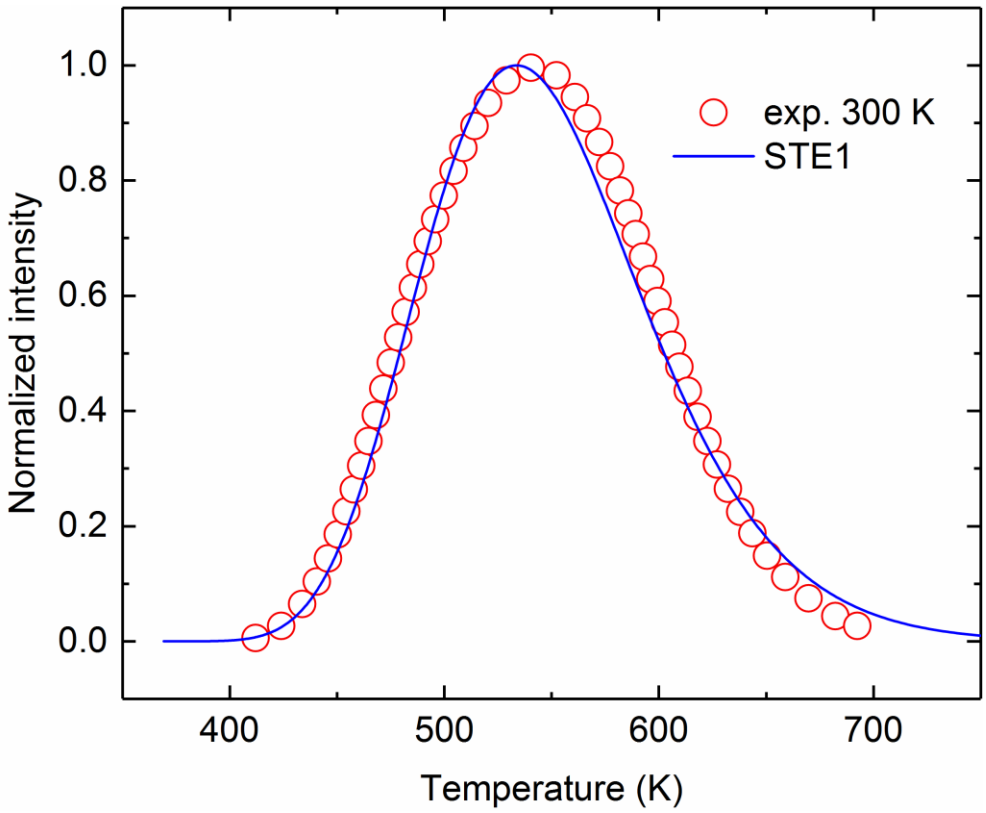

Figure 7. Theoretical photoluminescence spectrum of STE in Cs_4SnBr_6 compared with experiment[27].

In summary, we theoretically investigated the STE formation in four representative metal halide perovskites. We elucidate that the STE formation originates from the combination of low electronic dimensionality and soft atomic bonding. We observed multiple STE states for each material. The Jahn-Teller like STE is common among all the perovskites and is responsible for the observed broadband emission, whereby all the other STEs are active for non-radiative processes. The existence of the non-radiative active STEs competing with the Jahn-Teller like STE plays an

important role in determining the photoluminescence quantum efficiency. Therefore, enhance the formation of Jahn-Teller like STE and suppress the formation of the non Jahn-Teller like STE are viable approaches for improving the broadband emission quantum efficiencies of metal halide perovskites.

ASSOCIATED CONTENT

Supporting Information.

First-principles calculation (DFT, GW-BSE) details on STE and PL. This material is available free of charge via the Internet at http://pubs.acs.org.

Notes

The authors declare no competing financial interests.

ACKNOWLEDGMENT

This work was supported by the Center for Hybrid Organic Inorganic Semiconductors for Energy (CHOISE), an Energy Frontier Research Center funded by the Office of Basic Energy Sciences, Office of Science within the US Department of Energy. The method development was supported by the National Science Foundation under contract number DMR-1807818. Y. Y. acknowledges support from the Ohio Research Scholar Program. This research used the resources of the National Energy Research Scientific Computing Center, which is supported by the Office of Science of the U.S. Department of Energy under Contract No. DE-AC02-05CH11231.

REFERENCES

(1) Stranks, S. D.; Snaith, H. J. Metal-Halide Perovskites for Photovoltaic and Light-Emitting Devices. *Nat. Nanotechnol.* **2015**, *10* (5), 391–402.

(2) Hu, T.; Smith, M. D.; Dohner, E. R.; Sher, M. J.; Wu, X.; Trinh, M. T.; Fisher, A.; Corbett, J.; Zhu, X. Y.; Karunadasa, H. I.; et al. Mechanism for Broadband White-Light Emission from Two-Dimensional (110) Hybrid Perovskites. *J. Phys. Chem. Lett.* **2016**, *7* (12), 2258–2263.

(3) Smith, M. D.; Karunadasa, H. I. White-Light Emission from Layered Halide Perovskites. *Acc. Chem. Res.* **2018**, *51(3)*, 619-627.

(4) Yuan, Z.; Zhou, C.; Tian, Y.; Shu, Y.; Messier, J.; Wang, J. C.; van de Burgt, L. J.; Kountouriotis, K.; Xin, Y.; Holt, E.; et al. One-Dimensional Organic Lead Halide Perovskites with Efficient Bluish White-Light Emission. *Nat. Commun.* **2017**, *8*, 14051.

(5) Hayashi, T.; Kobayashi, T.; Iwanaga, M.; Watanabe, M. Exciton Dynamics Related with Phase Transitions in $CsPbCl_3$ Single Crystals. *J. Lumin.* **2001**, *94–95*, 255–259.

(6) Mao, L.; Guo, P.; Kepenekian, M.; Hadar, I.; Katan, C.; Even, J.; Schaller, R. D.; Stoumpos, C. C.; Kanatzidis, M. G. Structural Diversity in White-Light-Emitting Hybrid Lead Bromide Perovskites. *J. Am. Chem. Soc.* **2018**, *140* (40), 13078–13088.

(7) Luo, J.; Wang, X.; Li, S.; Liu, J.; Guo, Y.; Niu, G.; Yao, L.; Fu, Y.; Gao, L.; Dong, Q.; et al. Efficient and Stable Emission of Warm-White Light from Lead-Free Halide Double Perovskites. *Nature* **2018**, *563* (7732), 541–545.

(8) Luo, J.; Li, S.; Wu, H.; Zhou, Y.; Li, Y.; Liu, J.; Li, J.; Li, K.; Yi, F.; Niu, G.; et al. $Cs_2AgInCl_6$ Double Perovskite Single Crystals: Parity Forbidden Transitions and Their Application For Sensitive and Fast UV Photodetectors. *ACS Photonics* **2018**, *5* (2), 398–405.

(9) Volonakis, G.; Haghighirad, A. A.; Milot, R. L.; Sio, W. H.; Filip, M. R.; Wenger, B.; Johnston, M. B.; Herz, L. M.; Snaith, H. J.; Giustino, F. $Cs_2InAgCl_6$: A New Lead-Free

Halide Double Perovskite with Direct Band Gap. *J. Phys. Chem. Lett.* **2017**, *8* (4), 772–778.

(10) Zhou, J.; Xia, Z.; Molokeev, M. S.; Zhang, X.; Peng, D.; Liu, Q. Composition Design, Optical Gap and Stability Investigations of Lead-Free Halide Double Perovskite $Cs_2AgInCl_6$. *J. Mater. Chem. A* **2017**, *5* (29), 15031–15037.

(11) Pelle, F.; Jacquier, B.; Denis, J. P.; Blanzat, B. Optical Properties of $Cs_2NaBiCl_6$. *J. Lumin.* **1978**, *17* (1), 61–72.

(12) Cortecchia, D.; Neutzner, S.; Kandada, A. R. S.; Mosconi, E.; Meggiolaro, D.; De Angelis, F.; Soci, C.; Petrozza, A. Broadband Emission in Two-Dimensional Hybrid Perovskites: The Role of Structural Deformation. *J. Am. Chem. Soc.* **2017**, *139* (1), 39–42.

(13) Booker, E. P.; Thomas, T. H.; Quarti, C.; Stanton, M. R.; Dashwood, C. D.; Gillett, A. J.; Richter, J. M.; Pearson, A. J.; Davis, N. J. L. K.; Sirringhaus, H.; et al. Formation of Long-Lived Color Centers for Broadband Visible Light Emission in Low-Dimensional Layered Perovskites. *J. Am. Chem. Soc.* **2017**, *139* (51), 18632–18639.

(14) Li, Y. Y.; Lin, C. K.; Zheng, G. L.; Cheng, Z. Y.; You, H.; Wang, W. D.; Lin, J. Novel 〈110〉−Oriented Organic-Inorganic Perovskite Compound Stabilized by N-(3-Aminopropyl)Imidazole with Improved Optical Properties. *Chem. Mater.* **2006**, *18* (15), 3463–3469.

(15) Thirumal, K.; Chong, W. K.; Xie, W.; Ganguly, R.; Muduli, S. K.; Sherburne, M.; Asta, M.; Mhaisalkar, S.; Sum, T. C.; Soo, H. Sen; et al. Morphology-Independent Stable White-Light Emission from Self-Assembled Two-Dimensional Perovskites Driven by Strong Exciton–Phonon Coupling to the Organic Framework. *Chem. Mater.* **2017**, *29* (9), 3947–3953.

(16) Wang, S.; Yao, Y.; Kong, J.; Zhao, S.; Sun, Z.; Wu, Z.; Li, L.; Luo, J. Highly Efficient White-Light Emission in a Polar Two-Dimensional Hybrid Perovskite. *Chem. Commun.*

2018, *54* (32), 4053–4056.

(17) Yangui, A.; Pillet, S.; Bendeif, E. E.; Lusson, A.; Triki, S.; Abid, Y.; Boukheddaden, K. Broadband Emission in a New Two-Dimensional Cd-Based Hybrid Perovskite. *ACS Photonics* **2018**, *5* (4), 1599–1611.

(18) Wu, Z.; Ji, C.; Sun, Z.; Wang, S.; Zhao, S.; Zhang, W.; Li, L.; Luo, J. Broadband White-Light Emission with a High Color Rendering Index in a Two-Dimensional Organic–inorganic Hybrid Perovskite. *J. Mater. Chem. C* **2018**, *6* (5), 1171–1175.

(19) Dohner, E. R.; Hoke, E. T.; Karunadasa, H. I. Self-Assembly of Broadband White-Light Emitters. *J. Am. Chem. Soc.* **2014**, *136* (5), 1718–1721.

(20) Dohner, E. R.; Jaffe, A.; Bradshaw, L. R.; Karunadasa, H. I. Intrinsic White-Light Emission from Layered Hybrid Perovskites. *J. Am. Chem. Soc.* **2014**, *136* (38), 13154–13157.

(21) Yangui, A.; Garrot, D.; Lauret, J. S.; Lusson, A.; Bouchez, G.; Deleporte, E.; Pillet, S.; Bendeif, E. E.; Castro, M.; Triki, S.; et al. Optical Investigation of Broadband White-Light Emission in Self-Assembled Organic-Inorganic Perovskite $(C_6H_{11}NH_3)_2PbBr_4$. *J. Phys. Chem. C* **2015**, *119* (41), 23638–23647.

(22) Mao, L.; Wu, Y.; Stoumpos, C. C.; Wasielewski, M. R.; Kanatzidis, M. G. White-Light Emission and Structural Distortion in New Corrugated Two-Dimensional Lead Bromide Perovskites. *J. Am. Chem. Soc.* **2017**, *139* (14), 5210–5215.

(23) Du, K. Z.; Tu, Q.; Zhang, X.; Han, Q.; Liu, J.; Zauscher, S.; Mitzi, D. B. Two-Dimensional Lead(II) Halide-Based Hybrid Perovskites Templated by Acene Alkylamines: Crystal Structures, Optical Properties, and Piezoelectricity. *Inorg. Chem.* **2017**, *56* (15), 9291–9302.

(24) Mao, L.; Wu, Y.; Stoumpos, C. C.; Traore, B.; Katan, C.; Even, J.; Wasielewski, M. R.; Kanatzidis, M. G. Tunable White-Light Emission in Single-Cation-Templated Three-

Layered 2D Perovskites $(CH_3CH_2NH_3)_4Pb_3Br_{10-x}Cl_x$. *J. Am. Chem. Soc.* **2017**, *139* (34), 11956–11963.

(25) Smith, M. D.; Jaffe, A.; Dohner, E. R.; Lindenberg, A. M.; Karunadasa, H. I. Structural Origins of Broadband Emission from Layered Pb–Br Hybrid Perovskites. *Chem. Sci.* **2017**, *8* (6), 4497–4504.

(26) Yin, J.; Zhang, Y.; Bruno, A.; Soci, C.; Bakr, O. M.; Brédas, J. L.; Mohammed, O. F. Intrinsic Lead Ion Emissions in Zero-Dimensional Cs_4PbBr_6 Nanocrystals. *ACS Energy Lett.* **2017**, *2* (12), 2805–2811.

(27) Benin, B. M.; Dirin, D. N.; Morad, V.; Wörle, M.; Yakunin, S.; Rainò, G.; Nazarenko, O.; Fischer, M.; Infante, I.; Kovalenko, M. V. Highly Emissive Self-Trapped Excitons in Fully Inorganic Zero-Dimensional Tin Halides. *Angew. Chemie - Int. Ed.* **2018**, *57* (35), 11329–11333.

(28) Wu, G.; Zhou, C.; Ming, W.; Han, D.; Chen, S.; Yang, D.; Besara, T.; Neu, J.; Siegrist, T.; Du, M.-H.; et al. A One-Dimensional Organic Lead Chloride Hybrid with Excitation-Dependent Broadband Emissions. *ACS Energy Lett.* **2018**, *3* (6), 1443–1449.

(29) Xiao, Z.; Meng, W.; Wang, J.; Mitzi, D. B.; Yan, Y. Searching for Promising New Perovskite-Based Photovoltaic Absorbers: The Importance of Electronic Dimensionality. *Mater. Horiz.* **2017**, *4* (2), 206–216.

(30) Song, K. S.; Williams, R. T. *Self-Trapped Excitons*; Optical Sciences; Springer New York: New York, NY, 2008; Vol. 138.

(31) Alkauskas, A.; Lyons, J. L.; Steiauf, D.; Van de Walle, C. G. First-Principles Calculations of Luminescence Spectrum Line Shapes for Defects in Semiconductors: The Example of GaN and ZnO. *Phys. Rev. Lett.* **2012**, *109* (26), 267401.

(32) Huang, K.; Rhys, A. Theory of Light Absorption and Non-Radiative Transitions in F-Centres. *Proc. R. Soc. London. Ser. A. Math. Phys. Sci.* **1950**, *204* (1078), 406–423.